

Detecting Gravitational Waves from Test-Mass Bodies Orbiting a Kerr Black Hole with P-approximant Templates.

Edward K. Porter

Dept. of Physics, Montana State University, Bozeman, 59717, MT, USA.

E-mail: porter@physics.montana.edu

Abstract. In this study we apply post-Newtonian (T-approximants) and resummed post-Newtonian (P-approximants) to the case of a test-particle in equatorial orbit around a Kerr black hole. We compare the two approximants by measuring their *effectualness* (i.e. larger overlaps with the exact signal), and *faithfulness* (i.e. smaller biases while measuring the parameters of the signal) with the exact (numerical) waveforms. We find that in the case of prograde orbits, T-approximant templates obtain an effectualness of ~ 0.99 for spins $q \leq 0.75$. For $0.75 < q < 0.95$, the effectualness drops to about 0.82. The P-approximants achieve effectualness of > 0.99 for all spins up to $q = 0.95$. The bias in the estimation of parameters is much lower in the case of P-approximants than T-approximants. We find that P-approximants are both effectual and faithful and should be more effective than T-approximants as a detection template family when $q > 0$. For $q < 0$ both T- and P-approximants perform equally well so that either of them could be used as a detection template family. However, for parameter estimation, the P-approximant templates still outperforms the T-approximants.

1. Introduction

Stellar mass compact binaries consisting of double neutron stars (NS), double black holes (BH) or a mixed binary consisting of a neutron star and a black hole, are the primary targets for a direct first detection of gravitational waves (GW) by interferometric detectors, LIGO [1], VIRGO [2], GEO600 [3], and TAMA [4]. Under radiation reaction the orbit of a binary slowly decays, emitting a signal whose amplitude and frequency increases with time and is termed a “chirp” signal. While it is believed that there is a greater population of NS-NS binaries [5, 6, 7, 8, 9], it is the BH-BH binaries that are the strongest candidates for detection since they can be seen from a greater volume, about two orders-of-magnitude greater than NS-NS binaries [5, 10].

In order to detect such sources one employs the method of matched filtering [11]. The effectiveness of matched filtering depends on how well the phase evolution of the waveform is known. Even tiny instantaneous differences, as low as one part in 10^3 in the phase of the true signal that might be present in the detector output and the template that is used to dig it out could lead to a cumulative difference of several radians since one integrates over several hundreds to several thousands of cycles. In view of improving the signal-to-noise ratio for inspiral events there has been a world-wide effort in accurately computing the dynamics of a compact binary and the waveform it emits or to use phenomenologically defined detection template families [12, 13, 14].

There have been parallel efforts on using two different approximation schemes: On the one hand the post-Newtonian (PN) expansion of Einstein’s equations has been used to treat the dynamics of two bodies of comparable masses with and without spin, in orbit around each other. This approximation is applicable when the velocities involved in the system are small but there is no restriction on the ratio of the masses [15, 16, 17, 18, 19, 20, 21]. On the other hand, black hole perturbation theory has been used to compute the dynamics of a test particle in orbit around a spin-less or spinning black hole. Black hole perturbation theory does not make any assumptions on the velocity of the components, but is valid only in the limit when the mass of one of the bodies is much less than the other [22, 23, 24, 25, 26, 27].

The post-Newtonian approximation is a perturbative method which expands the equations of motion, binding energy and GW flux as a power series in v/c , where v is a typical velocity in the system and c is the speed of light. At present, the PN expansion for the case of comparable-masses is known to order $\mathcal{O}(v^6)$ [20] and $\mathcal{O}(v^7)$ [21], for the energy and flux functions, respectively.

As previously stated, black hole perturbation theory makes no assumptions about the orbital velocity of the components, but does restrict their masses. One assumes that a test particle of mass μ is in orbit about a central BH of mass M such that $\mu \ll M$. Assuming this restriction is satisfied we have an analytical expression for the energy. However, no analytical expression has been worked out for the gravitational wave flux emitted by such a system. Using black hole perturbation theory, the most recent series approximation was calculated to $\mathcal{O}(v^{11})$ by Tagoshi, Tanaka and Sasaki [27]. For a test particle in circular orbit about a Kerr black hole, the most recent progress is a series approximation to $\mathcal{O}(v^8)$, by Tagoshi, Tanaka, Shibata and Sasaki [28, 29].

Several authors [27, 30, 31, 32, 33] have shown that the convergence of both post-Newtonian approximation and black hole perturbation theory is too slow to be useful

in constructing accurate templates. More recently, Damour, Iyer and Sathyaprakash (hereafter DIS) showed for the case of a test-mass in orbit about a Schwarzschild BH, that by using properly defined energy and flux functions that have better analytical properties, combined with Padé techniques, it was possible to take the existing series expansion and improve its convergence properties [33]. The new approximation in which Padé approximants of new energy and flux functions are used to derive improved templates is called P-approximant. While in general, more templates are needed for P-approximant templates to cover the same volume of parameter space [34], the extra computational cost is preferred for the increased performance in P-approximants.

In this paper we will extend the P-approximant technique to the case of a test particle orbiting a Kerr black hole. The reason for focusing on test-mass systems is that we can use the exact numerical fluxes [35] from black hole perturbation theory with which to compare our results and thereby reliably demonstrate the usefulness of the technique.

2. The Gravitational Waveform.

In the stationary phase approximation the Fourier transform for positive frequencies reads [36, 37, 38, 39]

$$\tilde{h}(f) \equiv \int_{-\infty}^{\infty} h(t) \exp(2\pi i f t) dt = \frac{2\eta m \mathcal{C}}{d} \frac{v^2}{\sqrt{\dot{f}}} e^{i[\psi(f) - \frac{\pi}{4}]}, \quad (1)$$

where $m = m_1 + m_2$, $\eta = m_1 m_2 / m^2$, \mathcal{C} is a constant amplitude coefficient, d is the distance to the source, and, since $h(t)$ is real, $\tilde{h}(-f) = \tilde{h}^*(f)$. Also, $v = (\pi m f)^{1/3}$, \dot{f} is the time-derivative of the instantaneous gravitational wave frequency evaluated at the stationary point given by,

$$\dot{f} = -\frac{3v^2}{\pi m^2} \frac{F(v)}{E'(v)}, \quad (2)$$

where F is the gravitational wave flux function, $E'(v)$ is the derivative of the orbital energy function with respect to v , i.e. $E'(v) = dE/dv$, and the evolution of the phase of the Fourier transform in the stationary phase approximation is given by solving following set of coupled 1st order differential equations

$$\frac{d\psi}{df} - 2\pi t = 0, \quad \frac{dt}{df} + \frac{\pi m^2}{3v^2} \frac{E'(f)}{F(f)} = 0. \quad (3)$$

3. Gravitational Binding Energy and Flux Functions

We can see from Equation (3) that the phase of the gravitational wave depends both on the energy and flux functions of the binary system. In the test-mass case we have an exact expression for the energy $E(v)$, but only a series representation for the flux $F(v)$. Numerically, for the test mass case, the flux has been computed exactly. Since our aim is to draw conclusions on how effective P-approximants are in the comparable mass case, wherein one has only a Taylor expansion of the flux, we construct P-approximants of the flux and compare it with the numerical results. Padé approximation can be thought of as an operator P_M^N that acts on a polynomial $\sum_{k=0}^n a_k v^k$ to define a rational function $P_M^N = \sum_{k=0}^N A_k v^k / (1 + \sum_{k=1}^M B_k v^k)$ such that the $N + M + 1$ coefficients in the rational polynomial on the right hand side is

the same as the $n + 1$ Taylor coefficients on the left hand side. By setting $N = M + \epsilon$ with $\epsilon = 0, 1$, we can define two types of Padé approximants: These are the super-diagonal, $P_M^{M+\epsilon}$, and sub-diagonal, $P_{M+\epsilon}^M$, approximants. Normally, the sub-diagonal approximants are preferred over super-diagonal approximants. This is because when $M = N + \epsilon$ the rational function can be re-expanded as a continued fraction which has the property that as we go to each new order of the power series only one new coefficient needs to be calculated. Conversely, with the super-diagonal approximants, we would have to re-calculate all the A 's and B 's in the above equation as we go to higher orders in the Taylor expansion. This means that the sub-diagonal Padé approximants are more *stable* and if we see a trend of convergence in the coefficients the addition of a term is not likely to spoil this convergence.

3.1. The Orbital Energy.

In the case of both Schwarzschild and Kerr black holes we have an exact expression for the orbital energy of a test particle in a circular orbit around the parent black hole. For a black hole of mass M the energy E in terms of the dimensionless magnitude of velocity $v \equiv \sqrt{M/r}$, r being is the radial coordinate in the Boyer-Lindquist coordinates, takes the form [40]

$$E(v, q) = \eta \frac{1 - 2v^2 + qv^3}{\sqrt{1 - 3v^2 + 2qv^3}}. \quad (4)$$

where q is a dimensionless spin parameter given in terms of the spin angular momentum J of the black hole by $q \equiv J/M^2 \equiv a/M$, with a spin angular momentum per unit mass in the Kerr metric.

3.2. Post-Newtonian flux function

For a test-particle in a circular equatorial orbit, the post-Newtonian expansion of the flux function has been calculated up to $\mathcal{O}(v^{11})$ in the case of a Schwarzschild BH [27], and to $\mathcal{O}(v^8)$ in the case of a Kerr BH [28, 29]. The general form of the flux function in both these cases is given by the expression

$$F_{T_n}(x; q) = F_N(x) \left[\sum_{k=0}^n a_k(q)x^k + \ln(x) \sum_{k=6}^n b_k(q)x^k + \mathcal{O}(x^{n+1}) \right], \quad (5)$$

where $F_N(x) = \frac{32}{5}\eta^2 x^{10}$ is the dominant *Newtonian* flux function. Here, x is the magnitude of the invariant velocity parameter observed at infinity which is related to the angular frequency Ω by $x = (M\Omega)^{1/3}$. The relation between the parameter x and the local linear speed v in Boyer-Lindquist coordinates is given by

$$x(v, q) = v [1 - qv^3 + q^2v^6]^{1/3}, \quad (6)$$

which reduces, in the Schwarzschild limit, to $x = v$.

3.3. *P*-approximant of the flux function

In order to prepare the series representation of the flux for creating the Padé approximation, it is convenient if we factor out the logarithmic terms. We can then write Equation (5) as

$$F_{T_n}(x) = F_N(x) \left[1 + \ln \left(\frac{x}{x_{iso}} \right) \sum_{k=6}^n l_k x^k \right] \left[\sum_{k=0}^n c_k x^k \right], \quad (7)$$

where the new coefficients c_k and l_k are functions of the old coefficients a_k and b_k . As in Reference [33] the log-terms have been “normalized” using the value of the velocity parameter at the LSO; this helps in reducing the importance of the log-terms. x_{lso} is found by substituting $v_{lso} = \sqrt{M/r_{lso}}$ into Equation (6), where [40]

$$r_{lso}^{\pm}(q) = M \left[3 + z_2(q) \mp \sqrt{[3 - z_1(q)] [3 + z_1(q) + 2z_2(q)]} \right], \quad (8)$$

where

$$z_1(q) = 1 + (1 - q^2)^{\frac{1}{3}} \left[(1 + q)^{\frac{1}{3}} + (1 - q)^{\frac{1}{3}} \right], \quad z_2(q) = \sqrt{3q^2 + z_1^2}, \quad (9)$$

and the $+$ ($-$) sign corresponds to prograde (retrograde) orbits. We create the factored flux function, $f_{T_n}(x)$ by the operation $f_{T_n} \equiv (1 - x/x_{pole}) F_{T_n}$, where x_{pole} is obtained in the same way as x_{lso} but by using [40, 41]

$$r_{pole}^{\pm}(q) = 2M \left[1 + \cos \left[\frac{2}{3} \cos^{-1}(\mp q) \right] \right]. \quad (10)$$

Factoring out the pole also helps to alleviate the problem arising from the absence of the linear term in the PN expansion of the flux. (Note that $a_1 = 0$ in both the Schwarzschild and Kerr cases.) If we write the expression in full we obtain

$$f_{T_n}(x) = F_N(x) \left[1 + \ln \left(\frac{x}{x_{lso}} \right) \sum_{k=6}^n l_k x^k \right] \left[\sum_{k=0}^n f_k x^k \right], \quad (11)$$

where $f_0 = c_0$ and $f_k = c_k - c_{k-1}/x_{pole}$, $k = 1, \dots, n$,

We can now construct a new flux function by constructing the polynomial expansion of the inverse of the flux function and construct the Padé approximant of the resulting polynomial. We call the approximant constructed this way as *Inverse*- or *I*-Padé approximant because it is obtained from the Taylor expansion of the *inverse* of the flux function $f(v)$ in Equation (11). The Inverse Padé approximant of flux is defined by

$$f_{IP_n}(x) \equiv F_N^{-1}(x) \left[1 - \ln \left(\frac{x}{x_{lso}} \right) \sum_{k=6}^n l_k x^k \right] P_{m+\epsilon}^m \left[\sum_{k=0}^n d_k x^k \right], \quad (12)$$

where the coefficients d_k in the Taylor expansion are defined by $\sum_{k=0}^n d_k x^k \equiv (\sum_{k=0}^n f_k x^k)^{-1}$. We call the flux function constructed in this manner *P*-approximant. Thus, we define the *Inverse P*-approximant as,

$$F_{IP_n}(x) = \left[\left(1 - \frac{x}{x_{pole}} \right) f_{IP_n}(x) \right]^{-1}. \quad (13)$$

4. Effectualness and Faithfulness of T- and P-Approximants

We shall address the performance of the approximants in extracting the exact waveform in two ways: The *effectualness* of the templates measured in terms of the maximum overlap they can achieve with the exact waveform when the parameters of the approximant are varied in order to achieve a good match. The *faithfulness* of the approximant templates measured in terms of the systematic errors in the estimation of parameters while detecting exact waveforms.

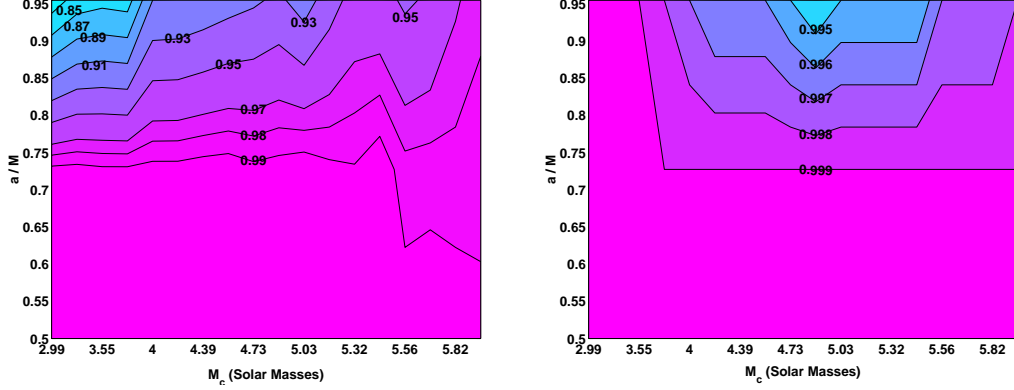


Figure 1. The maximized prograde overlaps for T-approximant (left) and P-approximant (right) templates at the x^8 approximation. Each system consists of a $1.4 M_\odot$ NS inspiralling into a central BH of mass ranging from 10-50 M_\odot .

4.1. Overlaps and fitting factor

We define the scalar product of two waveforms h and g by

$$\langle h | g \rangle = 2 \int_0^\infty \frac{df}{S_h(f)} \left[\tilde{h}(f) \tilde{g}^*(f) + \tilde{h}^*(f) \tilde{g}(f) \right], \quad (14)$$

where the $*$ denotes complex conjugate and $\tilde{h}(f)$, $\tilde{g}(f)$ are the Fourier transforms of $h(t)$, $g(t)$. For initial LIGO, the one-sided noise power spectral density (PSD) from the design study [1] is given by [39]

$$S_h(f) = 9 \times 10^{-46} [0.52 + 0.16x^{-4.52} + 0.32x^2] \text{ Hz}^{-1}, \quad (15)$$

where $x \equiv f/f_k$, and $f_k = 150 \text{ Hz}$ is the “knee-frequency” of the detector. We take the PSD to be infinite below the lower frequency cutoff of $f_{\text{low}} = 40 \text{ Hz}$. For two normalized waveforms, or signal vectors, the scalar product returns the cosine of the angle between them and is normally referred to as the *overlap*. For detection of signals what is more important is the *fitting factor* FF : As each template is a function of the parameters λ^μ , the fitting factor is defined as the maximum overlap obtained by varying the parameters of the template (or the approximate waveform) relative to the exact waveform:

$$FF = \max_{\lambda^\mu} O(\lambda^\mu). \quad (16)$$

If two waveforms are a perfect match then their overlap is unity. In the case of circular equatorial orbits of a test mass around a central black hole, the wave is parameterized by the set $\lambda^\mu = (t_0, \Phi_0, m, \eta, q)$. Maximization over t_0 is achieved by simply computing the correlation of the template with the data in the frequency domain followed by the inverse Fourier transform. It was pointed out [42, 43] that the maximum of the overlap of the data with a template over Φ_0 can be computed using just two templates – an *in-phase* and a *quadrature-phase* template.

Using a zero-phase un-normalized waveform, $\tilde{h}_0 = \tilde{h}(\Phi_0 = 0)$, we generate two orthonormalized waveforms according to $H_0 = \tilde{h}_0/|\tilde{h}_0|$ and $H_{\pi/2} = iH_0$, which is explicitly orthogonal to the in-phase template. The (square of the) maximum of the

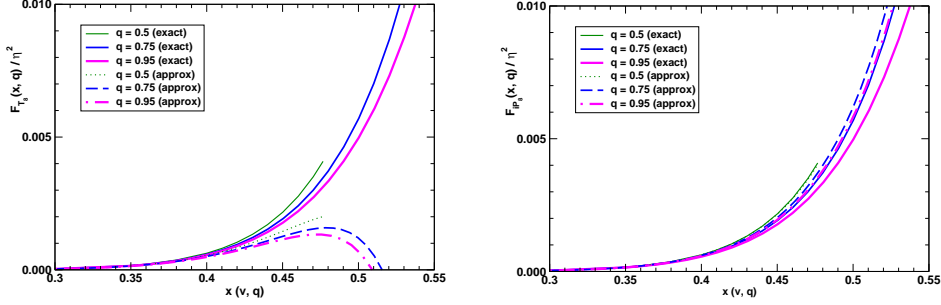


Figure 2. The 4-PN T-approximant (left) and P-approximant (right) analytical flux function for spins of $q = 0.5, 0.75$ and 0.95 against the numerical fluxes for the same spin values.

overlap over Φ_0 is given by the sum-of-squares of the overlap of the signal with the in-phase and quadrature-phase templates:

$$\max_{\Phi_0} (O) = \sqrt{\langle H_0 | h^X \rangle^2 + \langle H_{\pi/2} | h^X \rangle^2}, \quad (17)$$

where h^X denotes the “exact” waveform. Once this is done, we use a maximization routine to find the optimal values of the parameters (m, η, q) .

In this study, as we are working in the test-mass approximation, we assume that our system is composed of objects with a small mass ratio. For concreteness we assume that the system comprises a $1.4M_\odot$ NS inspiralling into a central BH of varying spin magnitude and mass. Beginning with a central BH of $10M_\odot$, we work our way upward to a $50M_\odot$ BH. We will also look at the limiting case of a 10-10 M_\odot equal-mass system. Strictly speaking, the formulas for energy and flux functions used in this study are not applicable to the comparable mass case since we have neglected the finite mass correction terms in these quantities. However, the results of such a study should give us an indication of how strong are the relativistic corrections, as opposed to finite-mass corrections, in the case of comparable masses. In all cases we vary the spin magnitude of the central BH from $q = -0.95$ to 0.95 . Since the main focus in this study is test-mass approximation we shall be interested in errors in estimating the chirp-mass, $\mathcal{M} = m\eta^{3/5}$, in addition to the spin magnitude of the central BH. In view of economy we shall only present the results for the highest PN order available, namely $\mathcal{O}(x^8)$ order. In all cases our fiducial *exact* signal h^X will be that obtained by using the exact expression for the energy in Equation (4) and the exact numerical fluxes generated using black hole perturbation theory [35], and the template will be the approximate waveform constructed using the exact expression for the energy, as before, and an approximate expression for the flux.

4.2. Prograde Orbits – Effectualness

For T-approximants – Figure 1, left panel – maximizing over all parameters gives fitting factors of $FF \geq 0.98$ at all mass ranges for the test-mass systems up to a spin of $q = 0.75$. Between 0.75 and $q = 0.95$, the T-approximant templates begin to perform badly and the fitting factors drop to $FF \sim 0.82$. For the equal-mass case – Figure 5 – the templates once again achieve fitting factors of $FF \geq 0.99$ up to a spin of $q = 0.75$,

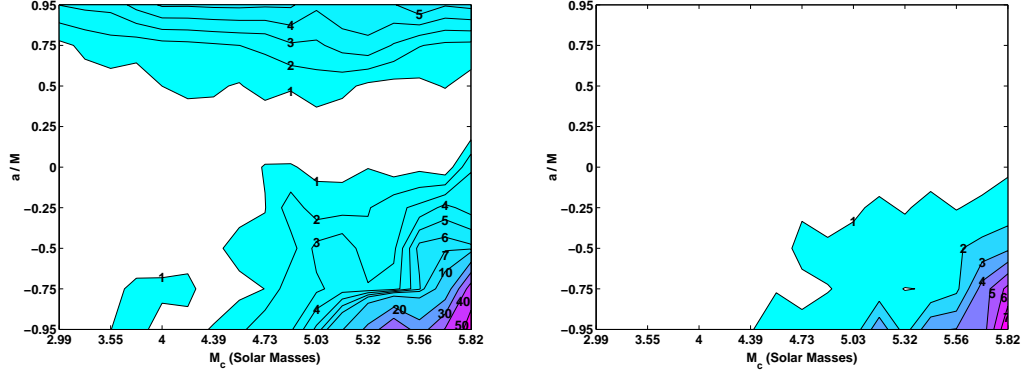


Figure 3. The percentage error in the estimation of the chirp-mass, \mathcal{M} , for T-approximant (left) and P-approximant (right) templates at the x^8 approximation.

but fall off at higher spin magnitudes achieving a fitting factor of ~ 0.98 at $q = 0.95$. We should point out that these results do not properly convey just how bad the 4-PN T-approximant template actually performs. In the left hand panel of Figure 2, we plot the PN approximation for the flux function against the numerical fluxes at spins of $q = 0.5, 0.75$ and 0.95 . These have corresponding values of $x_{lso} \approx 0.48, 0.54$ and 0.66 . We can see that the flux function at $q = 0.75$ and 0.95 become negative long before the LSO is reached. This means that as we go to higher and higher spins, we can model less and less of the waveform. For $q \leq 0.6$ we can model the waveform up to the LSO. However, for $q > 0.6$ this we have to stop the waveform generation at a cutoff velocity of $x_{cut} \approx 0.5$. Therefore, the fitting factors beyond $q = 0.75$ completely overestimate the performance of the T-approximant template.

If we now focus on the right hand panel of Figure 2, we see the true power of the P-approximant templates. The 4-PN template suffers none of the divergences that effect the T-approximants. We therefore generate all templates up to the LSO or 2 kHz, whichever is reached first. We can see from the right panel of Figure 1 that the P-approximant templates achieve fitting factors of > 0.99 at all spin values. For the equal-mass case – Figure 5 – the P-approximant templates achieve fitting factors of $FF \geq 0.995$ at all mass and spin levels. This demonstrates that in the case of prograde orbits, the P-approximant templates are clearly more robust, even at high spin magnitudes of $q = 0.95$.

4.3. Prograde Orbits – Faithfulness

In Figure 3 we have plotted the percentage bias in the estimation of the chirp-mass for both T- (left panel) and P-approximant (right panel) templates. From Figure 3, left panel, it is clear that for T-approximants the bias in \mathcal{M} varies between 0 – 5%. Comparing the left and right panels of Figure 3 we find that the P-approximant templates (right panels) are more faithful with the percentage bias being less than 1% in general.

In Figure 4 we present the percentage bias in the estimation of the spin magnitude of the central BH. We find that for both approximants we have to endure a large bias in q . Once again the P-approximant templates are more faithful. For T-approximants the bias varies between 5 and 90%, while for P-approximants it lies between 2 and 10%.

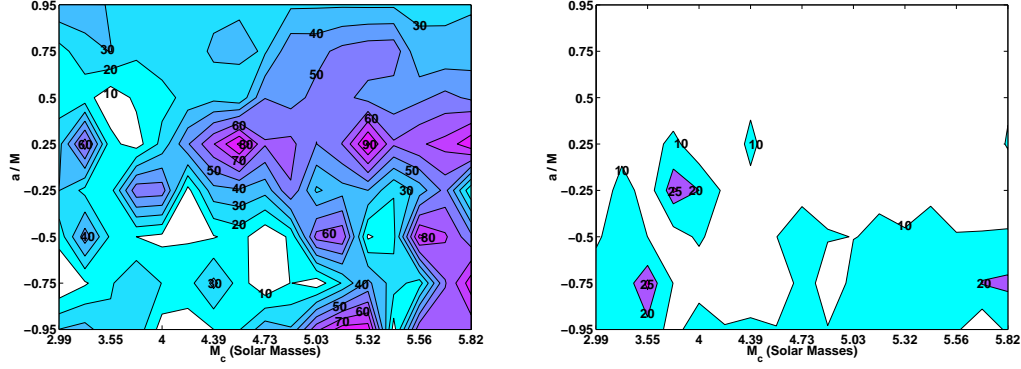


Figure 4. The percentage error in the estimation of the spin parameter, q , for T-approximant (left) and P-approximant (right) templates at the x^8 approximation.

From the middle and bottom Sections of Figure 5, it is clear that even in the equal mass case the bias in the estimation of both parameters is greater for T-approximant templates than P-approximants. It is therefore clear that in the case of prograde orbits, P-approximant templates must be used in any detection strategy.

4.4. Retrograde Orbits – Effectualness

In the case of retrograde orbits both templates achieve fitting factors of $FF \geq 0.99$ regardless of the spin magnitude and the chirp mass. There is no surprise here: The retrograde waveforms are still well within the adiabatic regime and are, therefore, modelled well by both templates. From a purely detection point of view, unlike the prograde case, there is no obvious benefit from employing P-approximant templates. For the equal mass system too there is not much difference in the fitting factors of the two families of templates with the exact signal.

4.5. Retrograde Orbits – Faithfulness

The benefit of using P-approximant templates for retrograde motion is only observed when we consider parameter extraction. Referring to the bottom portions of the two panels in Figure 3, we note that the T-approximants perform well at all spins for $3.0 \leq \mathcal{M}/M_\odot \leq 4.5$, with a bias of less than 1% in the estimation of \mathcal{M} . Beyond this, there is in general a bias of $> 2\%$. As we approach the extreme retrograde case the bias rises to as much as 55%. The P-approximants perform in a similar manner. The bias in the region $3 \leq \mathcal{M}/M_\odot \leq 4.5$ is again in general less than 1%. The error does again increase as we head towards the extreme test-mass range, but in this case it reaches a maximum value of 8% as opposed to the 55% seen in the case of the T-approximants.

The error in estimating q reaches a maximum of 80% for T-approximants and 25% for P-approximants. This is consistent with the results presented in Reference [28, 29] where it was shown that the PN approximation waveforms perform worse in the retrograde case. Now, referring once more to the equal mass case, the P-approximant templates outperform their T-approximant counterparts. Even with this, we must again conclude that while on the surface there is no clear case for using P-approximant

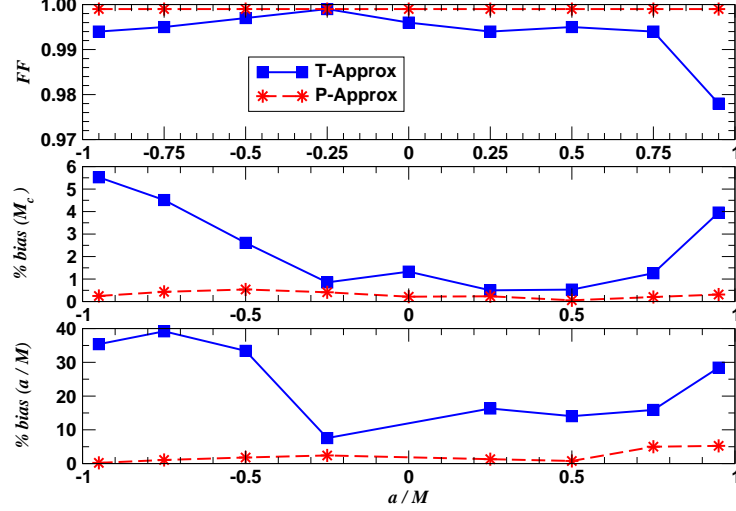


Figure 5. The fitting factors for a 10-10 M_\odot binary - without the finite mass correction terms - for T and P-approximant templates (top). The percentage error in the estimation of the chirp-mass for T and P-approximant templates (middle). The percentage error in the estimation of the spin of the central black hole for T and P-approximant templates (bottom).

templates in searching for retrograde motion systems, they should be used because of the lower bias incurred in the estimation of parameters.

5. Conclusions

We have applied P-approximant templates to the case of a NS orbiting Kerr BHs of varying mass and spin. Using a signal waveform constructed from the exact expression for the orbital energy and numerical fluxes from black hole perturbation theory, we were able to compare the performance of T and P-approximant templates. In the case of retrograde, Schwarzschild and prograde orbits, not only did the P-approximants gave better and more reliable fitting factors, they also gave smaller biases in the estimation of parameters. We also saw the true power of the P-approximant templates in that we were able to generate templates right up to the LSO. This is something that was not possible with the T-approximant templates due to the approximation for the flux function becoming negative before the LSO is reached. While not being completely correct due to the fact that we omitted the finite-mass correction terms, we also saw that the P-approximant templates gave the best performance when in the equal-mass case.

It is clear that for the type of systems examined in this paper, namely equatorial test-mass circular orbits in Kerr, P-approximant templates are to be preferred over their PN counterparts in both detection and measurement for prograde systems. For retrograde systems, while the T-approximants can be used for detection purposes, the P-approximants are superior when it comes to parameter estimation.

Acknowledgments

The author would like to thank B.S. Sathyaprakash, M. Shibata, T. Damour and B. Iyer.

References.

- [1] Abromovici A et al., *Science* **256**, 325 (1992)
- [2] Caron B et al, *Class. Quantum Grav.* **14**, 1461, (1997).
- [3] Willke B et al, *Class. Quantum Grav.* **19**, 1377, (2002).
- [4] Kuroda K et al in *Gravitational Waves : Sources and Detectors*, ed. by Cinfolini I and Fidecaro F, pg. 100 (World Scientific, 1997)
- [5] Grishchuk L P, Lipunov V M, Postnov K A, Prokhorov M E and Sathyaprakash B S, *Phys. Usp.* **44**, 1 (2001)
- [6] Phinney E, *Astrophys. J.* **380**, L17 (1991)
- [7] Narayan R, Piran T and Shemi A, *Astrophys. J.* **379**, L17 (1991)
- [8] Stairs I H et al., *Astrophys. J.* **505**, 352 (1998)
- [9] Belczynski K, Kalogera V and Bulik T, *Astrophys. J.*, **572** 407 (2001). astro-ph/0111452.
- [10] Postnov K A and Prokhorov M E, *Binary Black Hole Formation and Mergings*, in proceedings of the XXXIV Rencontres de Moriond "Gravitational waves and experimental Gravity", January 23-30, 1999, astro-ph/9903193.
- [11] Helstrom C W, *Statistical Theory of Signal Detection* (Pergamon Press, London 1968)
- [12] Buonanno A, Chen Y, and Vallisneri M, *Phys. Rev. D* **67**, 024016 (2003).
- [13] Buonanno A, Chen Y, and Vallisneri M, *Phys. Rev. D* **67**, 104025 (2003).
- [14] Pan Y, Buonanno A, Chen Y, and Vallisneri M, *Phys. Rev. D* **69**, 104017 (2004).
- [15] Blanchet L, Damour T, Iyer, B R, Will C M and Wiseman A G, *Phys. Rev. Lett.* **74**, 3515 (1995)
- [16] Blanchet L, Damour T and Iyer, B R, *Phys. Rev. D* **51**, 5360 (1995)
- [17] Will C M and Wiseman A G, *Phys. Rev. D* **54**, 4813 (1996)
- [18] Blanchet L, Iyer, B R, Will C M and Wiseman A G, *Class. Quantum Grav.* **13**, 575 (1996)
- [19] Blanchet L, *Phys. Rev. D* **54**, 1417 (1996)
- [20] Damour T, Jaranowski P and Schäfer G, *Phys. Rev. D* **63**, 044021 (2001); de Andrade V C, Blanchet L and Faye G, *Class. Quantum Grav.* **18**, 753, (2001).
- [21] Blanchet L, G. Faye, Iyer B R and Joquet B, *Phys. Rev. D* **65**, 061501 (2002); Blanchet L, Iyer B R and Joquet B, *Phys. Rev. D* **65**, 064005 (2002)
- [22] Poisson E, *Phys. Rev. D* **47**, 1497 (1993)
- [23] Cutler C, Finn L S, Poisson E and Sussman G J, *Phys. Rev. D* **47**, 1511 (1993)
- [24] Tagoshi H and Nakamura T, *Phys. Rev. D* **49**, 4016 (1994)
- [25] Sasaki M, *Prog. Theor. Phys.* **92**, 17 (1994)
- [26] Tagoshi H and Sasaki M, *Prog. Theor. Phys.* **92**, 745 (1994)
- [27] T. Tanaka, Tagoshi H and Sasaki M, *Prog. Theor. Phys.* 1087 (1996)
- [28] M. Shibata, Sasaki M, Tagoshi H and T. Tanaka, *Phys. Rev. D* **51**, 1646 (1995)
- [29] Tagoshi H, M. Shibata, T. Tanaka and Sasaki M, *Phys. Rev. D* **54**, 1439 (1996)
- [30] Cutler C et al, *Phys. Rev. Lett.* **70**, 2984 (1993)
- [31] Poisson E, *Phys. Rev. D* **52**, 5719 (1995)
- [32] Poisson E, *Phys. Rev. D* **55**, 7980 (1997)
- [33] Damour T, Iyer B R and Sathyaprakash B S, *Phys. Rev. D* **57**, 885 (1998)
- [34] Porter E K, *Class. Quantum Grav.* **19**, 4343, (2002)
- [35] Shibata M (Private communication).
- [36] Thorne K S, *Gravitational Radiation*, in Hawking S W and Israel W (eds), *300 Years of Gravitation* (Cambridge Uni. Press, Cambridge)
- [37] Sathyaprakash B S and Dhurandhar S V, *Phys. Rev. D* **44**, 3819 (1991)
- [38] Dhurandhar S V, Watkins J and Schutz B F, *Fourier transform of a coalescing binary signal* (Unpublished preprint)
- [39] Damour T, Iyer B R and Sathyaprakash B S, *Phys. Rev. D* **62**, 084036 (2000)
- [40] Bardeen J M, Press W H and Teukolsky S A, *Astrophys. J.* **178**, 374 (1972)
- [41] S. Chandrasekhar, *The Mathematical Theory of Black Holes* (Oxford Uni. Press, New York, 1983)
- [42] Schutz B F in *The Detection of Gravitational Radiation*, ed. by D. Blair (Cambridge Uni. Press, Cambridge 1989)
- [43] Dhurandhar S V and Sathyaprakash B S, *Phys. Rev. D* **49**, 1707 (1994)